ADVANCED HEALTHCARE MATERIALS
www.advhealthmat.de

PEI-Engineered Lipid@PLGA Hybrid Nanoparticles for Multimodal Delivery of Antigens and Immune Adjuvants to the Respiratory Mucosa

*Susy Brusco, Gemma Conte, Annunziata Corteggio, Teresa Silvestri, Andrea Spitaleri, Paola Brocca, Agnese Miro, Fabiana Quaglia, Ivana d'Angelo, Luciana D'Apice, Paola Italiani, Gabriella Costabile, and Francesca Ungaro**

Antigen delivery via respiratory mucosal surfaces is an interesting needle-free option for vaccination. Nonetheless, it demands for the design of especially tailored formulations. Here, lipid/poly(lactic-co-glycolic) acid (PLGA) hybrid nanoparticles (hNPs) for the combined delivery of an antigen, ovalbumin (Ova), and an adjuvant, synthetic unmethylated cytosine-phosphate-guanine oligodeoxynucleotide (CpG) motifs, is developed. A panel of Ova/CpG-loaded lipid@PLGA hNPs with tunable size and surface is attained by exploiting two lipid moieties, 1,2 distearoil-sn-glycero-3-phosphoethanolamine-poly(ethylene glycol) (DSPE-PEG) and monophosphoryl lipid A (MPLA), with or without polyethyleneimine (PEI). It is gained insights on the lipid@PLGA hNPs through a combination of techniques to analytically determine the specific moiety on the surface, the spatial distribution of the components and the internal structure of the nanoplatforms. The collected results suggest that PEI plays a role of paramount importance not only in promoting in vitro antigen escape from lysosomes and enhancing antigen cross-presentation, but also in determining the arrangement of the moieties in the final architecture of the hNPs. Though multicomponent PEI-engineered lipid@PLGA hNPs turn out as a viable strategy for delivery of antigens and adjuvant to the respiratory mucosa, tunable nanoparticle features are achievable only through the optimal selection of the components and their relative amounts.

1. Introduction

The main lesson learned from the recent COVID-19 pandemic is that immunization through vaccination is the best defence against serious, preventable and sometimes deadly contagious diseases. Vaccines trigger the immune system by simulating pathogen infection and prompting the body to mount a defensive response against the actual pathogen. Generally, the host's immune system is straightaway activated after humoral (i.e., antibody formation) and cellular (i.e., cell-mediated) stimuli. However, the response strongly depends on the site of induction of the immunity, whether systemic or mucosal.[1]

Considering that mucosal surfaces constitute the interface between the body and the external environment, they are the port of entry of infective agents into the body, consequently playing a central role in immune surveillance, and protection against infection. Indeed, inducing immunity at the sites of pathogen entry has the unique potential to prevent the infection from getting established.[2] Therefore, an increasing

S. Brusco, G. Conte, T. Silvestri, A. Miro, F. Quaglia, G. Costabile, F. Ungaro
Department of Pharmacy
University of Napoli Federico II
Via D. Montesano 49, Napoli 80131, Italy
E-mail: ungaro@unina.it

The ORCID identification number(s) for the author(s) of this article can be found under https://doi.org/10.1002/adhm.202402688

DOI: 10.1002/adhm.202402688

A. Corteggio, L. D'Apice, P. Italiani
Institute of Biochemistry and Cell Biology
National Research Council
Via Pietro Castellino 111, Napoli 80131, Italy

A. Spitaleri, P. Brocca
Department of Medical Biotechnologies and Translational Medicine
University of Milano
Via F.lli Cervi 93, Segrate (MI) 20054, Italy

I. d'Angelo
Di.S.T.A.Bi.F.
University of Campania Luigi Vanvitelli
Caserta 81100, Italy

research interest has been devoted to mucosal vaccination to elicit both systemic immune response and mucosal immunity.[3]

Among the mucosal routes of administration, vaccination through the respiratory mucosa could be an interesting strategy for both preventive and therapeutic immunization.[4,5] In fact, it allows direct interaction of the antigen with nasopharynx-associated lymphoid tissue (NALT) or the bronchus-associated lymphoid tissue (BALT), excellent sites for stimulating not only the mucosal but also the systemic immunity, through activation of B- and T-cells.[6] Once activated, B and T cells can migrate either to other mucosal tissues or to secondary systemic lymphoid tissues and induce a strong systemic immunization. In contrast, the immunization by parental routes can only induce weak mucosal immunity.[2]

Although inhaled vaccines offer some advantages, their development for mucosal immunization still faces significant hurdles, such as: i) identifying the optimal region of the respiratory tract for protective immunogenicity; ii) finding the dose of antigen able to stimulate protective immunity, while avoiding tolerance induction; iii) developing economic devices compatible with preclinical and clinical administration.[4,7] Finally, an appropriate design of the vaccine formulation, that can also work as adjuvant, is desirable. Indeed, the unique anatomic, physiological and immunological features of the respiratory tract demand for different vaccination strategies as compared to conventional parenteral route.[5]

The approval of mRNA lipid nanoparticles for the prevention of severe acute respiratory syndrome coronavirus 2 (SARS-CoV-2) infection represented a milestone for vaccines leveraging on nanotechnologies. The so called "nanovaccines" exploit nanotechnologies to overcome biological barriers to antigen release, therefore they represent an excellent opportunity to induce strong immune protection at mucosal surfaces.[8,9] Among the different nanoplatforms for delivery of antigens to respiratory mucosa, biocompatible and biodegradable polymeric nanoparticles (NPs) based on poly(lactic-co-glycolic) acid (PLGA) have sparked research interest.[10–12] PLGA-based NPs can in principle protect the antigen cargo from degradation and allow prolonged and specific co-delivery of antigen and immune adjuvants from a single platform, thus enhancing immunogenicity.[13–15]

To date, several attempts have been made to develop multimodal PLGA-based nanovaccines co-encapsulating antigens, as ovalbumin (Ova), and adjuvants, as non-methylated oligodeoxynucleotides containing cytosine-guanine-phosphate motifs (CpG)[16–18] or glycolipids, including monophosphoryl lipid A (MPLA).[18–20] In fact, toll-like receptors (TLR) agonists, as TLR4 and TLR9 ligands, might be highly beneficial as vaccine adjuvants due to the crucial role played by these receptors in modulating innate immunity and shaping the adaptive immune response.[21] Nonetheless, independently upon the co-entrapped adjuvant, data showed that NP composition and surface properties have an impact on the type and extension of induced immune responses.[11,22–24] Meanwhile, they can strongly affect the fate of the NP along the airways.

Several surface-engineering strategies have been proposed to improve the transport of NPs across the airway barriers, such as mucus. Hydrophilic materials, as poly(ethylene glycol) (PEG), have been firstly used to endow NPs with mucus-penetrating properties.[25,26] More recently, muco-inert and cell-penetrating core-shell hybrid NPs (hNPs) have been achieved by combining PLGA and lipids, exhibiting complementary characteristics of polymer NPs and liposomes.[26]

Here we designed and developed a multimodal inhalable nanovaccine comprising a PLGA core, containing OVA as model antigen and a CpG motif as adjuvant. Given the key role that NP surface plays in engaging with the biological environment, we explored the effect of different moieties as surface coating, thus obtaining a panel of lipid@PLGA hNPs. We tried i) 1,2 distearoil-sn-glycero-3-phosphoethanolamine-poly(ethylene glycol) (DSPE-PEG), to achieve mucus-penetrating DSPE-PEG@PLGA hNPs; ii) MPLA, to obtain both a mucoinert and immuno-responsive MPLA@PLGA hNPs. Finally, the addition of polyethyleneimine (PEI) was attempted to improve the efficiency of lipid@PLGA hNPs, as reported for conventional vaccines against infections and tumors.[27,28] The architecture of the resulting lipid@PLGA hNPs was investigated through a combination of analytical tests, which would help to verify the presence and to quantify the specific moiety on the surface, as well as through qualitative tests (i.e., SAXS) to gain information related to the spatial distribution of the components and the internal structure of the optimized nanoplatforms. The impact of lipid@PLGA hNP features on their interactions with mucin and mucus penetration was investigated. Finally, selected formulations were tested for: i) uptake studies on murine dendritic cells (DCs), ii) antigen presentation tests to B3Z OT-I hybridoma cells expressing a TCR that specifically recognize the OVA (257–264) (SIINFEKL) antigen.[29]

2. Experimental Section

2.1. Materials

Resomer RG 502H (uncapped PLGA 50:50, inherent viscosity 0.16 0.24 dL/g) was purchased from Evonik Industries AG (Germany). 1, 2-distearoyl-sn-glycero-3-phosphoethanolamine–poly (ethylene glycol)2000 (DSPE-PEG) was kindly gifted from Lipoid GmbH (Switzerland). Poly(ethylene glycol) methyl ether-block-poly(lactide-co-glycolide) (PEG-PLGA; PEG average Mn 5000 and PLGA Mn 5000; PEG average Mn 2000, PLGA Mn 3000), polyethylenimine (PEI; Mw 25 000 Da, branched, water-free), albumin from chicken egg white (lyophilized powder, ≥98% agarose gel electrophoresis), copper (II) sulphate, sodium chloride, sodium hydroxide, potassium chloride, and potassium phosphate monobasic were purchased from Merk Life Science S.r.l. (Italy). Synthetic monophosphoryl lipid A from *E. coli* (MPLA) and the synthetic oligonucleotide containing unmethylated CpG dinucleotides ODN 2395 (CpG) were bought from InvivoGen (Italy). RPMI 1640 and Fetal bovine serum (FBS) media were bought from Thermo Fisher Scientific Inc. (Italy). Ethanol 96% (v/v), dichloromethane (DCM) and all the other solvents were supplied by Carlo Erba reagents (Italy). Ultrapure water (UPW, type I) was achieved by a Purelab Option-Q system (Elga Labwater, Italy) and used throughout the study.

Table 1. Composition of the Ova-loaded hybrid nanoparticles (theoretical amounts for 10 mg of PLGA).

Formulation	Ova [mg]	CpG [mg]	MPLA [mg]	DSPE-PEG [mg]	PEI in w [mg]	PEI in o [mg]
Ova_MPLA@PLGA	0.225	–	0.10	–	–	–
Ova/CpG_MPLA@PLGA	0.225	0.025	0.10	–	–	–
Ova/CpG/PEI_{low}_MPLA@PLGA	0.225	0.025	0.10	–	0.032	–
Ova/CpG/PEI_{high}_MPLA@PLGA	0.225	0.025	0.10	–	3.50	–
Ova/CpG_MPLA@PLGA/PEI_{low}	0.225	0.025	0.10	–	–	0.032
Ova/CpG_MPLA@PLGA/PEI_{high}	0.225	0.025	0.10	–	–	3.50
Ova_DSPE-PEG@PLGA	0.225	–	–	0.50	–	–
Ova /CpG_DSPE-PEG@PLGA	0.225	0.025	–	0.50	–	–
Ova/CpG/PEI_{low}_DSPE-PEG@PLGA	0.225	0.025	–	0.50	0.032	–
Ova/CpG/PEI_{high}_DSPE-PEG@PLGA	0.225	0.025	–	0.50	3.50	–
Ova/CpG DSPE_PEG@PLGA/PEI_{low}	0.225	0.025	–	0.50	–	0.032
Ova/CpG_DSPE-PEG@PLGA/PEI_{high}	0.225	0.025	–	0.50	–	3.50

2.2. Quantitative Analysis of Ovalbumin and CpG

Ovalbumin (Ova) was quantified by either spectrophotometry or spectrofluorimetry with a multimode microplate reader GloMax™ (Promega Italia Srl, Italy). Colorimetric analysis of unlabelled Ova was performed using a Bradford protein assay reagent (Thermo Fisher Scientific, USA) according to the manufacturer's instructions. The linearity of the response at 660 nm was verified over the concentration range 0.02-0.45 µg/mL ($r^2 \geq 0.99$). Spectrofluorimetric analysis of labelled Ova-ATTO 594 was performed at $\lambda_{ex}/\lambda_{em}$ 520 nm/580–640 nm. The linearity of the response was verified over the concentration range 0.2-50 µg mL^{-1} ($r^2 \geq 0.99$).

CpG quantitation was performed using Quant-iT OliGreen reagent (Thermo Fisher Scientific, USA) according to the manufacturer's instructions. Spectrofluorimetric analysis of the samples was performed at $\lambda_{ex}/\lambda_{em}$ 480 nm/520 nm (GloMax™ Plate reader, Promega Italia Srl, Italy). The linearity of the response was verified over the concentration range 0.015-1 µg mL^{-1} ($r^2 \geq 0.99$).

2.3. Production of Lipid@PLGA Hybrid Nanoparticles

The lipid@PLGA hNPs were produced by a modified emulsion-solvent diffusion technique.[26,30,31] Briefly, a solution (200 µL) of Ova (2.5% w/w) and CpG (0.5% w/w) in UPW was emulsified under vortex mixing (Reax top, Heidolph, Germany to an organic phase) in an organic phase which consisted in PLGA-containing dichloromethane (DCM) with or without lipids (i.e., DSPE-PEG or MPLA). The emulsion was poured into 12.5 mL of ethanol (under magnetic stirring) and then diluted with 12.5 ml of UPW. To remove any residual organic solvent, the colloidal dispersion was rotary evaporated under vacuum at 37 °C to a final volume of 5 mL (Rotavapor, Heidolph VV 2000, Germany). Finally, lipid@PLGA hNPs were isolated by centrifugation at 7000 rpm for 20 min (Hettich Zentrifugen, Universal 16R), and resuspended in UPW at fixed concentration. When needed, PEI was added either to the aqueous phase or to the organic phase of the emulsion. The composition of the different hNP formulations was reported in **Table 1**.

2.4. Nanoparticle Characterization

After production, Ova-loaded lipid@PLGA hNPs were characterized for hydrodynamic diameter (D_H), polydispersity index (PDI) and zeta (ζ) potential. D_H and PDI were determined by dynamic light scattering (DLS) and ζ potential with electrophoretic light scattering (ELS) with a Zetasizer Nano ZS (Malvern Instruments Ltd, UK). For ELS measurements, hNP formulations were diluted in UPW and analysed. Results are reported as mean of three measurements on three different batches (n = 9) ± standard deviation (SD).

After hNP isolation by centrifugation, the supernatants underwent quantitative analysis for Ova and/or CpG contents (i.e., not encapsulated amounts) as described above. Given the total mass of antigen and/or adjuvant added to the formulation, the amounts of Ova and CpG loaded inside lipid@PLGA hNPs were evaluated indirectly by difference between the total and the not encapsulated amounts.[32] All the results are reported as actual loading (mg of Ova or CpG per 100 mg of lipid@PLGA hNPs) and encapsulation efficiency (actual loading/theoretical loading × 100) ± standard deviation (SD) of values derived from three measurements on three different batches (n = 9).

Optimised MPLA@PLGA and DSPE-PEG@PLGA were further characterized for morphology, size and particle concentration by Transmission Electron Microscopy (TEM) and Nanoparticle Tracking Analysis (NTA).

NTA measurements were performed on a NanoSight Pro (Malvern Panalytical Ltd, UK) equipped with a high sensitivity scientific CMOS camera and a 488 nm laser. Samples were prepared in 1 mL volume using UPW for NTA analysis, filtered through a 0.22 µm syringe filter immediately prior to use. Flow rate was set to 3 µL min^{-1}. Videos were recorded 5 time for each sample, 11.5 s each, at a controlled temperature of 25 °C. All analyses were performed using NS Xplorer software (Malvern, UK).

The morphology of the lipid@PLGA hNPs was evaluated by TEM with a FEI Tecnai G^2 S-TWIN microscope equipped with a FEI Eagle 4K camera. Sample analysis was performed upon air drying of 7 µL lipid@PLGA hNPs dispersions in water (10 mg/500 µL) mounted on 200 mesh copper grids coated with

carbon film (Ted Pella Inc., Nanovision, Italy). Before analysis, the NPs were stained with phosphotungstic acid (2%, w/v).

2.5. Surface Analysis of Nanoparticles

2.5.1. Fixed Aqueous Layer Thickness

Fixed aqueous layer thickness (FALT) was calculated by a conventional double layer model from ζ potential measurements (Nano ZS, Malvern Instruments, UK) of NP dispersions (0.5 mg mL^{-1}) in aqueous NaCl.[33] The slope of the linear regression achieved by plotting ln (ζ) versus k ($k = 3.3\ C^{0.5}$; where k^{-1} is the Debye length and C the molar concentration of NaCl) represents the thickness of the shell (nm). The results were expressed as nm ± standard deviation (SD) calculated on triplicate experiments.

2.5.2. Chromogenic MPLA Quantitation

MPLA quantification was performed by a Pierce Chromogenic Endotoxin Quant-Kit (Thermo Scientific, USA) according to the manufacturer's instructions. Briefly, the assay was performed on either lipid@PLGA hNPs (1 mg/100 µL) diluted in Endotoxin Free water (EFW- Thermo Fisher Scientific, USA) (*direct method*) or the respective supernatants recollected after the centrifugation phase (indirect method). The optical density (OD) of the samples at 405 nm was measured and the amount of MPLA calculated using a calibration in the range of 0.0625–1 µg ml^{-1} ($r^2 \geq 0.95$). The results were expressed as percent of MPLA adhered on hNP surface ± SD of triplicate experiments.

2.5.3. PEG Quantification with ELISA Assay

Quantitation of PEG on DSPE-PEG@PLGA hNPs surface was performed by enzyme-linked immunosorbent assay (ELISA) according to the manufacturer's procedure (Cloud Clone Corporation, USA). Ova/CpG PEG NPs and Ova/CpG DSPE-PEG NPs at concentration of 1 mg of /100 µL were tested for PEG content on DSPE-PEG@PLGA hNPs surface at wavelength of 450 nm (GloMax™ Plate reader, Promega Italia Srl, Italy). The calibration curve was achieved solubilizing PEG 2000 (0.5 µg mL^{-1}) in UPW at 5—10 °C for 2 h under magnetic stirring (the transmittance was measured to ensure the dissolution of PEG >95%). For quantitative measurements, the OD of the sample was compared to the corresponding calibration curve. The results were reported as percentage of PEG detected on nanoparticle surface ± SD of triplicate experiments.

2.5.4. PEI Quantification

PEI was quantified by a previously developed spectrophotometric assay upon complexation with copper (II).[34] PEI analysis was performed on the supernatants recollected after the centrifugation phase of the lipid@PLGA hNPs *(indirect method)*. Briefly, 0.5 ml of PEI-containing samples were buffered with an equal volume of 1 M acetic acid. The resulting solutions were diluted to 2 ml by means of acetate buffer and complexed with copper (II) in 0.1 M acetate buffer at pH 5.4 as reacting medium. The absorbance values at 285 nm were recorded and compared to the corresponding calibration curve. All the results were reported as actual loading (mg of PEI per 100 mg of nanoparticles) and encapsulation efficiency (actual loading/theoretical loading × 100) ± SD of triplicate experiments.

2.6. Differential Scanning Calorimetry

Thermoanalytical tests were carried out by a differential scanning calorimeter (DSC) (Q20, TA Instruments, USA), preliminarily calibrated with a pure indium standard. Briefly, lipid@PLGA hNPs were freeze-dried at 0.1 mbar and −80 °C (LyoQuest, Telstar Italy). Accurately weighted solid samples (1–2 mg) were placed in aluminium sealed pans and heated from 20 to 80 °C at a constant heating rate of 5 °C min^{-1}. Measurements were carried out under an inert nitrogen atmosphere and purged at a flow rate of 50 ml min^{-1}. An empty pan was used as a reference. The thermodynamic parameters, as enthalpy (ΔH) and glass transition temperature (T_g), were evaluated. The DSC analysis was performed firstly on the raw materials, as PLGA, Ova and PEI. Then the thermodynamics behavior of the hNP formulations was evaluated.

2.7. Small-Angle X-Ray Scattering (SAXS) Analysis

Small angle X-ray scattering (SAXS) measurements were performed at the Austrian SAXS beamline of ELETTRA synchrotron facility in Trieste, Italy and at the Id02 beamline of ESRF synchrotron facility in Grenoble (FR). For measurements at ELETTRA, a *Pilatus3 1 M* detector system was used with a sample-to-detector distance of 2.3 m to have a q-range from 1.06×10^{-1} to 6 nm^{-1} corresponding to the range of distances 1 to 60 nm in the direct space. For measurements at ESRF a Eiger2 4 M detector was used at two different sample to detector distances of 10 and 1 meters to cover the direct space interval of ≈1 µm -1 nm, with profitable overlapping. Flow through glass cells were used. Measurements have been performed at room temperature. Samples were measured at 10 mg mL^{-1} concentration in water. Empty capillaries and capillaries filled with water have been measured in the same conditions, for background subtraction. SAXS data have been treated applying SAXS utilities software[35] and analyzed SASFit[36] employing core multishell sphere form factor model[37] which provide the scattering length density profile of a multi-shell sphere, where the interface between each neighboring shells was described by the error function.

2.8. Molecular Dynamics Simulations

MD simulations were performed with the GROMACS software (http://www.gromacs.org/), version 2022.3, using CHARMM36M as force field, together with the explicit TIP3P water model and 51 K+ ions, which were added to neutralize the net charge of the system. The equilibration protocol consisted of a series of energy minimizations and short restrained MD runs in the NVT ensemble. This was followed by production

runs in the NPT ensemble at 303.15 K and pressure of 1 atm. Periodic boundary conditions, together with the Particle Mesh Ewald method to treat long-range interactions and a 2 fs time step were used. The starting 3D structure of ODN 2395 CpG was calculated using IsRNA and subsequently relaxed in 50 ns of all-atoms simulation. The structure of Ova was downloaded from PDB database (PDB ID 1UHG) and used as monomer. The Ova- CpG complex was calculated using ab initio docking protocol, exploiting Lightdock software based on the Glowworm Swarm Optimization (GSO) algorithm. MPLA was parametrized with CHARMM36M force field, using CHARMM-GUI web service. The system Ova- CpG-MPLA was build using gmx insert-molecules tool in ratio 1:1:10 mols. We conducted four separate molecular dynamics simulations, each lasting 200 ns, using the top four docked structures based on their scores. This resulted in a total simulation time of 0.8 µs. Finally, an additional 1.3 µs molecular dynamics simulation to assess the time scale of Ova-CpG complex formation was conducted. Analysis of the simulations were performed using in-house python script and gmx tools.

2.9. In Vitro Release Kinetics

Optimised lipid@PLGA hNPs underwent in vitro release studies in phosphate buffer at a pH of 7.2 (PBS; 120 mM NaCl, 2,7 mM KCl, 10 mM phosphate salt) at 37 °C. Briefly, experiments were carried out on a dispersion of NPs (1 mL, 2 mg/100 µl) in shaking water bath (LBS Aqua Pro, Grant Instruments Ltd, US). At scheduled time points, the samples were centrifuged at 7000 rpm for 20 min (Hettich Zentrifugen, Universal 16R) and the supernatants were tested for Ova and CpG content as described above. Experiments were carried out in triplicate and results expressed as cumulative release (%) ± SD.

2.10. Mucoadhesive Tendency of Nanoparticles

2.10.1. In Vitro Nanoparticle Interactions with Mucin

The interactions of optimized lipid@PLGA hNPs with mucin from porcine stomach (Type II, Merk KGaA, Germany) were investigated by the mucin-particle method as previously described.[36] Briefly, hNP dispersions (1 mg/50 µL) were diluted to 1 mg mL^{-1} in a saturated mucin solution in UPW (0.08% w/V) and incubated for 30 and 60 min at room temperature. Turbidimetric analyses were performed by measuring the absorbance (ABS) at 650 nm on a Shimadzu UV 1800 spectrophotometer (Shimadzu Italia S.r.l., Italy). hNP dispersions in UPW and the mucin dispersion were analysed as controls. The analyses were supported by DLS measurements of nanoparticle dispersion in mucin and water after 60 min of incubation (Nano ZS, Malvern Instruments, UK). All the experiments were performed in triplicate and the results expressed mean value ± SD.

2.10.2. In Vitro Transport of Nanoparticles Through Artificial Mucus

In vitro transport studies were performed on fluorescent lipid@PLGA hNPs prepared by a previously developed model based on Transwell multiwell plates.[31] Artificial mucus (AM) and simulated interstitial lung fluid (SILF) were prepared as previously reported.[39] For AM, 25 µL of sterile egg yolk emulsion, 25 mg of mucin from porcine stomach, Type II, 20 mg of DNA, 30 µL of aqueous DTPA (1 mg mL^{-1}), 25 mg NaCl, 11 mg KCl, and 100 µL of RPMI 1640 were added to 5 mL of water, and the dispersion was stirred until a homogenous mixture was obtained. A 1 L of SILF contains 0.095 g of magnesium chloride, 6.019 g of sodium chloride, 0.298 g of potassium chloride, 0.126 g of sodium phosphate dibasic, 0.063 g of sodium sulfate, 0.368 g calcium chloride dihydrate, 0.574 g of sodium acetate, 2.604 g of sodium bicarbonate, and 0.097 g of sodium citrate dihydrate. Briefly, 25 µL of hNP dispersions in water (10 mg ml^{-1}) were placed on top of an AM layer (75 µL) in a 6.5 mm Transwell insert with 8.0 µm pore polycarbonate membrane. The inserts were transferred in a 24-well plate containing 300 µL of SILF per well. At scheduled time intervals, the acceptor medium was withdrawn and centrifuged to isolate nanoparticles (9000 rcf for 20 min at 4 °C). The pellet was suspended in water, diluted 10x with 0.5 N NaOH and stirred for 1.5 h to degrade the lipid@PLGA hNPs. The amount of nanoparticles in the resulting solution was quantified by spectrofluorimetric analysis of $PLGA_{Rhod}$ at λ_{ex} 520 nm/λ_{em} 580–640 nm (GloMax™ Plate reader, Promega Italia Srl, Italy). Calibration curves were derived by analysing serial dilutions of a stock NPs dispersion degraded in 0.5 M NaOH. The linearity of the response was verified over the concentration range 5–100 µg mL^{-1} ($r^2 \geq 0.99$). All the experiments were performed in triplicate and the results expressed as percentage (%) of total NPs permeated over time ± SD.

2.11. In Vitro Cell Culture Studies

2.11.1. Cell Culture

B3Z hybridoma cells were cultured in RPMI 1640 (GIBCO) supplemented with 10% FCS, 100 U mL^{-1} penicillin, 100 µg mL^{-1} streptomycin 1% Glutamine, 1% Non-Essential amino-acids, 1% Sodium Pyruvate, 50 µM 2-Mercaptoethanol.

Bone Marrow derived dendritic cells differentiation: C57BL/6 (eight-week-old, female) were purchased from Charles River (Lecco, Italy) and housed at Animal House Facility of IGB-CNR under standard pathogen-free conditions, according to institutional guidelines. In accordance with the EU Directive for animal experiments 2010/63/EU, and authorized by Italian Ministry of Health (authorization number 7E58D.12 released on 5-20-2020), precursors for Bone Marrow-derived Dendritic Cells (BM-DCs) derivation were isolated from the tibiae of euthanized C57BL/6 mice. After cutting tibiae ends, bone marrow was flushed with ice-cold RPMI 1640 medium (Microgem). BM-DC precursors were washed twice with medium, and clusters of cells were disaggregated by pipetting. Cells were plated in RPMI 1640 medium supplemented with 10% foetal calf serum (FCS), 60 µg mL^{-1} penicillin, 100 µg mL^{-1} streptomycin, 1 mM sodium pyruvate and 50 µM 2-mercaptoethanol and with 200 U mL^{-1} recombinant murine granulocyte/macrophage colony-stimulating factor (GM-CSF, Peprotech, NJ, USA). GM-CSF was added on day 1,3 and 6 after plating, replacing the culture medium. Immature DCs were collected eight days later. For confocal microscopy experiments,

BM-DC differentiation was carried on after seeding BM-DC precursors on sterile glass coverslips in 24 well cell culture plate on day 1.

2.11.2. Uptake in Murine Dendritic Cells

BM-DCs, plated on glass coverslips at the density of 1×10^5cell, were treated with rhodamine labelled-nanoparticles loaded with Ova (10 ug mL^{-1}) at different time points (2, 6, and 24 h). At the end of the incubation, cells were fixed with 4% paraformaldehyde for 15 min, washed three times in PBS and then incubated in blocking solution [0.5% (w/v) BSA, 50 mM NH_4Cl in PBS, pH 7.4, 0.05% saponin] for 30 min at 25 °C. Cells were subsequently incubated with Anti-LAMP-1 antibody (PA1654A, Thermo Fisher Scientific; Invitrogen, Milan, Italy; 1:400), specific for lysosomal compartment, diluted in blocking solution O/N at 4 °C. After incubation with the Anti-LAMP-1, cells were washed three times in PBS and incubated with the secondary antibody diluted in blocking solution (AlexaFluor-488 conjugated, Thermo Fisher Scientific, Invitrogen, Milan, Italy; 1:400). Nuclei were stained with Hoechst 33 258. Finally, cells were washed 3 times in PBS and once in sterile water to remove salts. Coverslips were then mounted on glass-microscope slides with Mowiol (20 mg mowiol dissolved in 80 mL PBS). Images were taken using a Zeiss-LSM 700 confocal microscope. Optical confocal sections were taken at 1 Air Unit.

2.11.3. Antigen Presentation Tests in B3Z OT-I Hybridoma Cells

5×10^5/mL BM-DCs were incubated with nanoparticles loaded with 1, 5 or 10 µg mL^{-1} of Ovalbumin (in 0.1 mL $well^{-1}$ of complete medium). As a control, BM-DCs were incubated in medium alone. After overnight incubation, 5×10^5/well B3Z cells (OTI hybridoma line) in 0.1 mL $well^{-1}$ of complete medium was added for co-culture. After 40 hours co-culture, cell culture supernatant (0.1 mL $well^{-1}$) was collected and used for IL-2 detection by ELISA assay using the ELISA MAX™ Deluxe Set Mouse IL-2 (BioLegend) according to the manufacturer's instructions.[40–42] Supernatants of co-cultures were assayed in duplicate, and results are representative of two independent experiments.

2.12. Statistical Analysis

A two-way ANOVA and Bonferroni multiple comparison test were performed using GraphPad Prism 8. (GraphPad Software, Inc., San Diego, CA, USA). Statistical significance values were indicated as *p< 0.05; **p< 0.005; ***p< 0.0005; ****p< 0.0001.

3. Results and Discussion

3.1. Development of Lipid@PLGA Hybrid Nanoparticles for the Co-Delivery of Ovalbumin and CpG

In this work, multimodal PLGA-based nanovaccines for the combined release of a model antigen, namely Ovalbumin (Ova), and a vaccine adjuvant, the non-methylated oligodeoxynucleotides containing cytosine-guanine-phosphate motifs (CpG) have been successfully developed. The PLGA core was surface-modified with either Monophosphoryl lipid A (MPLA) or 1,2-dissteroylphosphatidylethanolapine (ethylene glycol) 2000 (DSPE-PEG), thus attaining lipid@PLGA hNPs. The lipid@PLGA hNPs were further engineered through the addition of branched polyethyleneimine (PEI) to facilitate the uptake of NPs in dendritic cells (DCs), as well as to promote the activation of the immune system (Table 1; **Figure 1**).

Pre-formulation studies were performed to select the lipid@PLGA hNP formulations to move forward. Acknowledging the crucial role played by particle size and surface properties in overcoming the barriers imposed by the respiratory system (i.e., mucus),[43] all formulations have been fully characterized in terms of size (D_H), PDI and ζ potential (**Figure 2**).

The DLS analysis show that Ova/CpG-loaded lipid@PLGA engineered at surface with either MPLA or DSPE-PEG were homogeneously dispersed (PDI ≤ 0.12), with a mean size lower than 250 nm and a negative surface charge of ≈ -30 mV (Figure 2). An increase of hNP size was apparent for Ova/CpG_DSPE-PEG@PLGA (D_H 223.3 ± 2.7 nm) as compared to Ova/CpG_MPLA@PLGA hNPs (D_H 186.3 ± 3.6), likely ascribable to PEG chains grafted on hNP surface.[44]

To exploit the full potential of PEI in the production of lipid@PLGA hybrid nanovaccines, different formulations were produced in terms of addition mode and amount of PEI included in the formulation. PEI was added either in the water phase or in the organic phase during the emulsion formation step, and the following amounts were considered: 0.032 and 3.5 mg for PEI_{low} and PEI_{high} formulations, respectively. Changes to the properties of the nanoplatforms after addition of branched PEI to the formulation were monitored (Figure 1A). Special emphasis was given to lipid@PLGA hNP surface charge. The positive charge of the polymer, in fact, is beneficial for cell uptake of the carrier as it allows the electrostatic interaction with the negative charges of the peptidoglycans on the cell membranes, thus favoring lipid@PLGA hNP internalization.[45,46] Except for Ova/CpG/PEI_{high}_MPLA@PLGA hNPs, the PDI and the mean size of lipid@PLGA hNPs increased when PEI was added to the Ova/CpG-containing water phase. Furthermore, independently on the amount of PEI added to the formulation, the surface charge was still strongly negative with ζ potential values as low as −30/-35 mV (Figure 2). Trying to achieve positively-charged lipid@PLGA hNPs, the attention was focused on lipid@PLGA hNP formulations achieved by addition of PEI in the organic phase. As shown in Figure 2A, the size of the lipid@PLGA hNPs tends to decrease by increasing the amount of PEI added to the formulation, with optimal values ≈160 nm for Ova/CpG_MPLA@PLGA/PEI_{high} (161.6 ± 30.5 nm) and Ova/CpG_DSPE-PEG@PLGA/PEI_{high} (156.8 ± 14.2 nm), as also confirmed by NTA measurements and TEM analyses (Figure 2B,C). All MPLA@PLGA/PEI and DSPE-PEG@PLGA/PEI hNPs appear like spherical and homogeneously dispersed with a PDI ≤0.12 and a Span-1. Notably, an inversion of the surface charge was evident for PEI_{high} formulations, which were characterized by a strongly positive ζ potential values (≈ +50 mV), indicating the presence of PEI on the surface, as suggested also by the ζ potential change as a function of

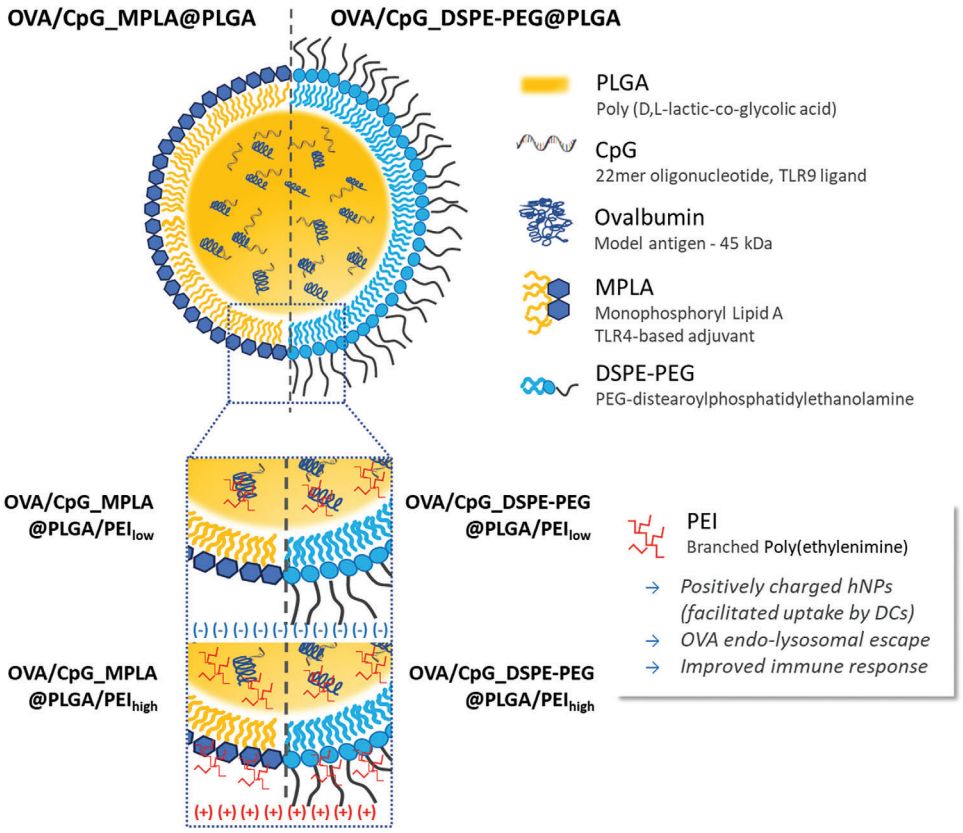

Figure 1. Schematic representation of Ova/CpG-loaded MPLA@PLGA and DSPE-PEG@PLGA hNPs.

the medium pH (Figure S1, Supporting Information). This hypothesis is further supported by results of PEI quantitation inside PEI_{high} formulations (**Table 2**). Indeed, only 45–58% of the initial amount of PEI added to the formulation was loaded in PEI_{low} lipid@PLGA hNPs (≈0.15 mg per 100 mg of lipid@PLGA hNPs). Contrariwise, PEI_{high} formulations are characterized by ≈93% of PEI associated to the lipid@PLGA hNPs, that is PEI actual loadings 150 folds higher than those measured for the corresponding PEI_{low} lipid@PLGA hNPs.

The determination of an adequate response by the immune system depends on the nature of the immunogenic components of the platform, with particular regard to the amounts of antigen/adjuvants encapsulated/released over time and the intracellular route of the internalized antigen.[37] The amounts of Ova and CpG entrapped inside lipid@PLGA hNPs are reported in Table 2. Depending upon the composition of the formulation, Ova was entrapped inside the lipid@PLGA hNPs with efficiencies ranging from 64% to 89%. In particular, the co-encapsulation of CpG exerted a beneficial effect on Ova entrapment efficiency inside MPLA@PLGA hNPs, with Ova/CpG_MPLA@PLGA showing a 23% increase in the encapsulated antigen compared to Ova_MPLA@PLGA (Table 2). In the

Table 2. Ova, CpG and PEI entrapment efficiencies inside MPLA@PLGA and DSPE-PEG@PLGA hNPs. All the results are reported as mean ± standard deviation (SD) of values derived from three measurements on three different batches (n = 9).

Formulation	Yields of production [% ± SD]	Ova actual loading[a)] [% ± SD]	CpG actual loading[a)] [% ± SD]	EE Ova [% ± SD]	EE CpG [% ± SD]	EE PEI [% ± SD]
Ova_MPLA@PLGA	63.6 ± 4.7	2.55 ±0.95	–	67.3 ± 1.1	–	–
Ova/CpG_MPLA@PLGA	59.0 ± 0.12	4.41 ± 0.12	0.40 ± 0.014	89.5 ± 2.6	93.8 ± 0.41	–
Ova/CpG_MPLA@PLGA/PEI_{low}	54.5 ± 4.24	2.90 ± 0.52	0.40 ± 0.073	69.0 ± 1.0	86.2 ± 0.24	45.8 ± 2.1
Ova/CpG_MPLA@PLGA/PEI_{high}	58.5 ± 4.2	3.12 ± 0.23	0.42 ± 0.031	81.0 ± 8.0	99.1 ± 0.12	93.4 ± 1.2
Ova_DSPE-PEG@PLGA	73.5 ± 3.5	1.95 ± 0.09	–	63.6 ± 0.7	–	–
Ova/CpG_DSPE-PEG@PLGA	64.5 ± 6.4	2.46 ± 0.24	0.38 ± 0.037	70.2 ± 4.2	97.6 ± 0.42	–
Ova/CpG_DSPE-PEG@PLGA/PEI_{low}	67.5 ± 3.5	2.14 ± 0.11	0.29 ±0.015	64.0 ± 3.9	78.9 ± 0.21	58.2 ± 5.4
Ova/CpG_DSPE-PEG@PLGA/PEI_{high}	84.0± 5.6	2.07 ± 0.21	0.30 ± 0.030	77.0 ± 3.1	99.5 ± 0.34	93.6 ± 2.1

[a)] Actual loadings are expressed as mg of encapsulated Ova or CpG per 100 mg of nanoparticles based on the yields of production. Ova theoretical loading was 2 mg/100 mg of nanoparticles.

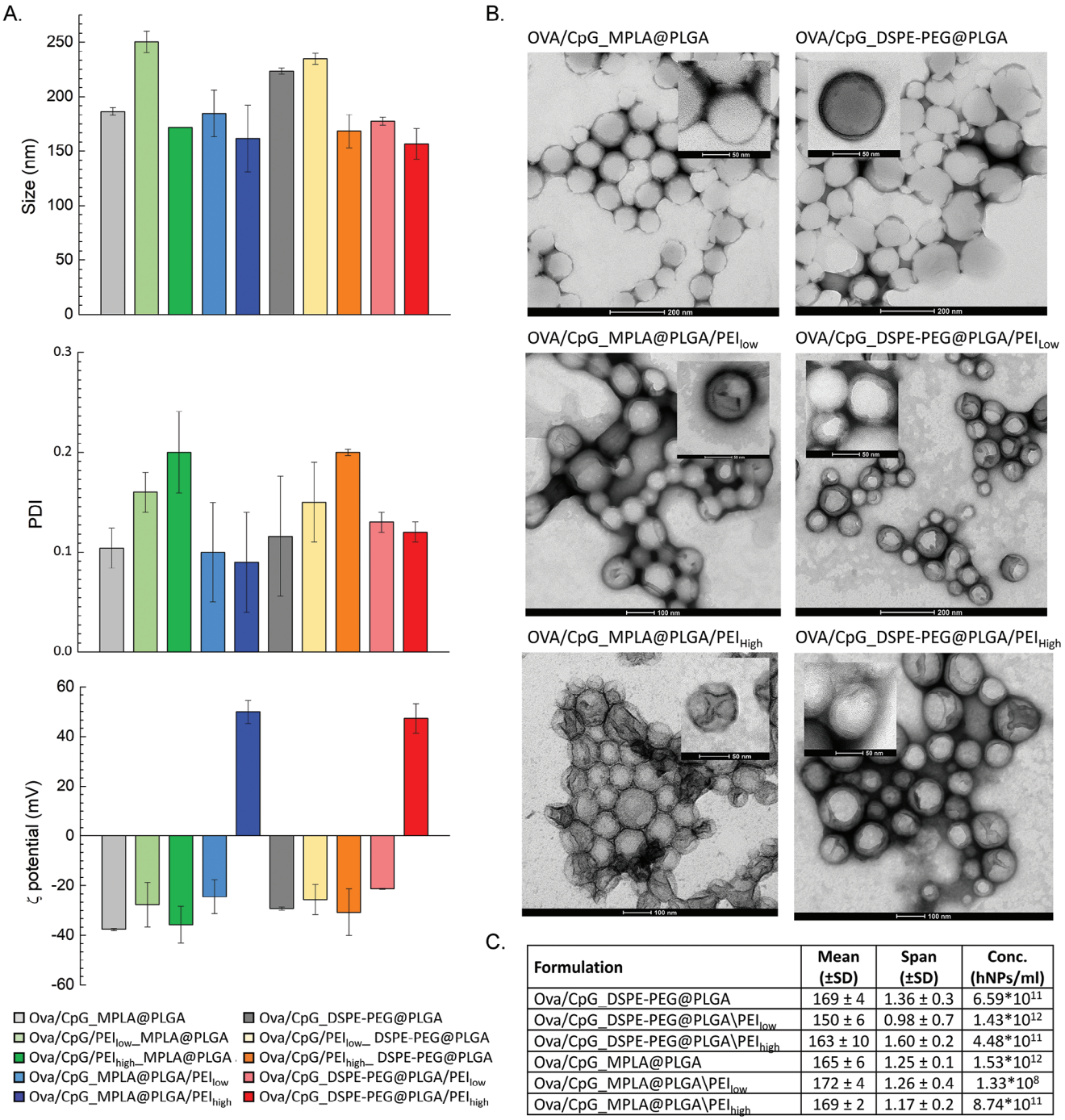

C.

Formulation	Mean (±SD)	Span (±SD)	Conc. (hNPs/ml)
Ova/CpG_DSPE-PEG@PLGA	169 ± 4	1.36 ± 0.3	$6.59*10^{11}$
Ova/CpG_DSPE-PEG@PLGA\PEI$_{low}$	150 ± 6	0.98 ± 0.7	$1.43*10^{12}$
Ova/CpG_DSPE-PEG@PLGA\PEI$_{high}$	163 ± 10	1.60 ± 0.2	$4.48*10^{11}$
Ova/CpG_MPLA@PLGA	165 ± 6	1.25 ± 0.1	$1.53*10^{12}$
Ova/CpG_MPLA@PLGA\PEI$_{low}$	172 ± 4	1.26 ± 0.4	$1.33*10^{8}$
Ova/CpG_MPLA@PLGA\PEI$_{high}$	169 ± 2	1.17 ± 0.2	$8.74*10^{11}$

Figure 2. Characterization of Ova/CpG-loaded MPLA@PLGA and DSPE-PEG@PLGA hNPs. A) Size, polydispersity index (PDI) and zeta potential of the different formulations. B) TEM images of optimized Ova/CpG-loaded hNPs. Field is representative of the formulation. C) NTA characterization. Mean, Span and Particle concentration (hNPs/ml) as calculated by the NTA software. Results are reported as mean of three measurements on three different batches (n = 9) ± standard deviation (SD).

same fashion, the addition of high amounts of PEI favorably affected CpG entrapment efficiency. This can be likely due to the electrostatic interactions occurring between the polycation and the oligonucleotide, as further supported by in vitro release studies (**Figure 3**).

In vitro release studies were performed to evaluate the ability of the lipid@PLGA hNPs to assist the release of Ova and CpG throughout time. In each case a typical biphasic release profile, consisting in a *burst*, followed by a controlled release of the loaded species lasting 1 week was observed for both Ova and

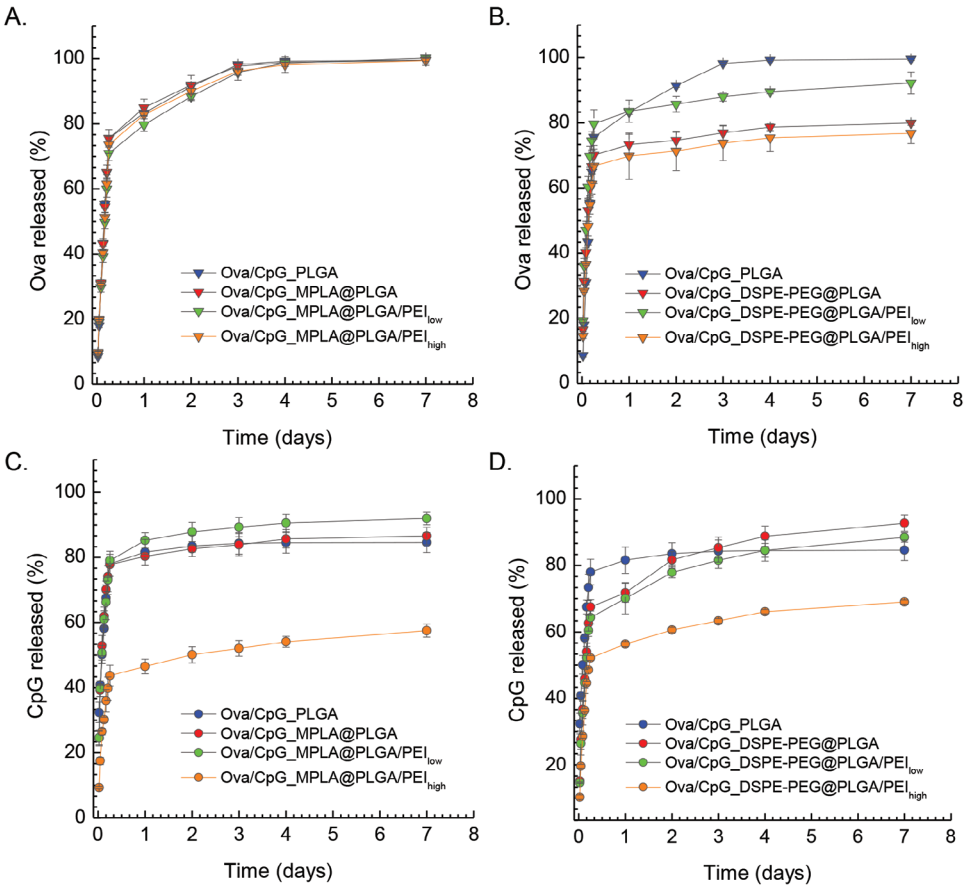

Figure 3. In vitro release profiles at pH 7.2 and 37 °C of Ova and CpG from MPLA@PLGA hNPs A and C) and DSPE-PEG@PLGA hNPs B and D). The release profiles of Ova and CpG from bare PLGA nanoparticles (Ova/CpG@PLGA) in the same experimental conditions are reported for comparison. Results are reported as mean of two measurements on three different batches (n = 6) ± standard deviation (SD).

CpG (Figure 3). If the first phase is likely ascribable to payload desorption from the surface, the second is mainly driven by the diffusion through the lipid@PLGA matrix. Nonetheless, differences in the release profiles of Ova from MPLA@PLGA and DSPE-PEG@PLGA hNPs were apparent (Figure 3A,B). In particular, the release of Ova from MPLA@PLGA hNPs is faster and complete (100% of the entrapped amount released after 1 week), while it slowed down in the case of DSPE-PEG@PLGA hNPs. In the latter case, by increasing the amount of PEI inside the formulation, the release rate decreased, with a percentage of 76.8 ± 3.14% of Ova released after 1 week. The effect of PEI addition inside the formulation was much more evident for CpG release kinetics (Figure 3C,D), indicating that a percentage as low as 60% of CpG is released from PEI_{high} formulation after 6 days. This can be reasonably ascribed to the establishment of electrostatic interactions between PEI and polyanionic CpG, as a consequence of PEI partitioning in the aqueous phase during the emulsification step.[47] These interactions, which have been recently demonstrated as a valuable tool to complex CpG in nanovaccine formulations,[48] reasonably give rise to macromolecular PEI/CpG polyplexes slowly diffusing from lipid@PLGA matrix.[47]

It can therefore be concluded that the addition of adequate amounts of PEI in Ova/CpG-loaded lipid@PLGA hybrid nanovaccines allows a clear improvement in the entrapment efficiency of both the antigen and the vaccine adjuvant, which are slowly released form the developed nanoplatforms. These results, along with the positive effects on size, PDI and potential ζ, prompt toward further investigation of the potential of Ova/CpG_MPLA@PLGA/PEI_{high} and Ova/CpG_DSPE-PEG@PLGA/PEI_{high} formulations for antigen presentation studies.

3.2. Insight into the Architecture of Ova/CpG Loaded Lipid@PLGA Hybrid Nanoparticles

The formulations optimized in terms of encapsulation efficiency/release rate of Ova and CpG have been further characterized for their surface properties, with regard to the composition and conformation of the shell, which are key to the modulation of nanovaccine interactions with the physiological environment and, therefore, to ensure its efficacy.

As for DSPE-PEG@PLGA hNPs, hydrophilic PEG chains grafted on particle surface are expected to generate a hydrated cloud with a large, excluded volume that prevents hNP interaction with proteins and other components of the physiological fluids.[44] When added, PEI chains reasonably contributes to the

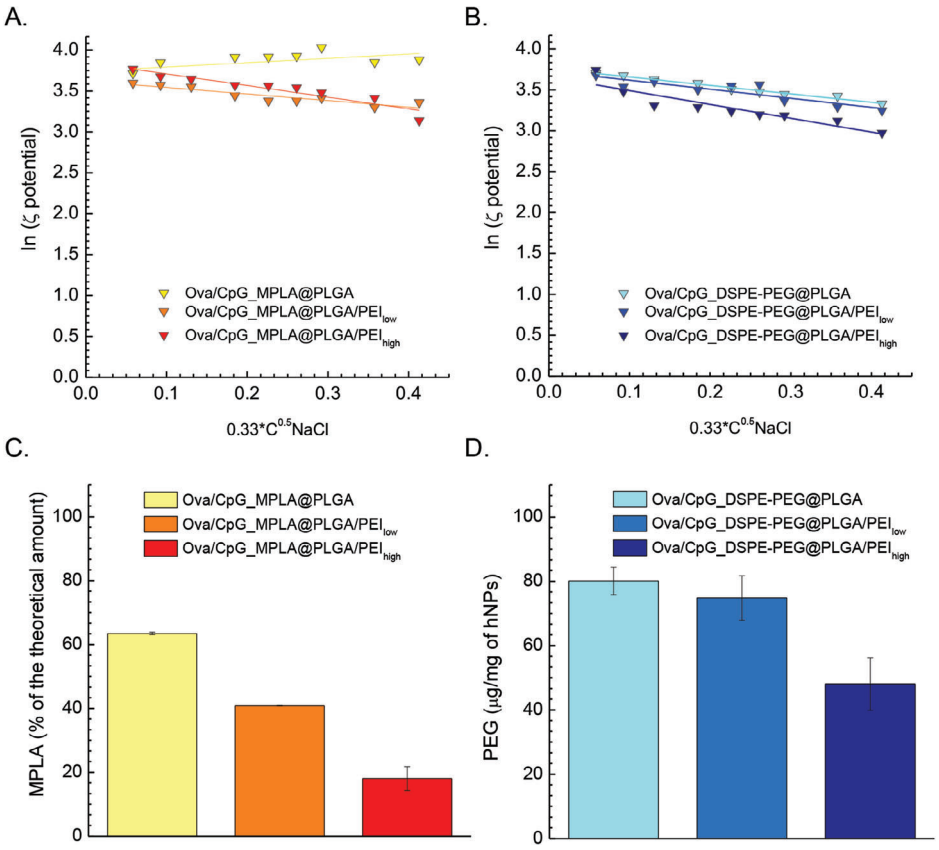

Figure 4. Surface analysis of Ova/CpG-loaded lipid@PLGA nanoparticles. A,B) FALT measurements of the shell thickness, derived from the slopes of the corresponding linear regressions. B) Percentage of MPLA associated to MPLA@PLGA hNPs. C) Amount of PEG quantified in DSPE-PEG@PLGA hNPs through ELISA. Results are reported as mean of two measurements on three different batches (n = 6) ± standard deviation (SD).

aqueous layer thickness.[49] Thus, FALT measurements were performed to verify the presence of the hydrophilic polymer shell covering hNPs and to evaluate how the lipids used as nanoparticle building blocks affect it. By plotting the ln ζ potential versus Debye-Huckel parameter, it is possible to derive the FALT (nm) from the slope of the curve.[50] As expected, unmodified Ova/CpG_MPLA@PLGA hNPs do not display a relevant FALT (0.58 ± 0.10 nm) (**Figure 4A**). According to the Gouy-Chapmann theory, the ζ potential of both PEI-engineered and PEGylated hNPs decreases as the ionic strength of the medium increases (as a result of the increasing NaCl concentration), more steeply for PLGA/PEI$_{high}$ as compared to PLGA and PLGA/PEI$_{low}$ formulations (Figure 4A,B). A 3-fold increase of FALT was observed for Ova/CpG_MPLA@PLGA/PEI$_{high}$ (1.42 ± 0.039 nm) as compared to Ova/CpG_MPLA@PLGA. Also, the FALT of Ova/CpG_DSPE-PEG@PLGA/PEI$_{high}$ (1.65 ± 0.062 nm) was ≈1.5-fold higher than Ova/CpG_DSPE-PEG@PLGA (1.03 ± 0.060 nm) hNPs, confirming a contribution of PEI to the hydrated shell, as suggested also by the positive surface charge (Figure 2A).

The presence of PEG associated to DSPE-PEG@PLGA hNPs was corroborated by quantitative analysis through ELISA (Figure 4C). The assay relies on a competitive inhibition enzyme immunoassay technique, based on microplates pre-coated with a monoclonal antibody specific to PEG. A competitive inhibition reaction was launched between PEG-containing hNPs with the antibody specific to PEG, thus allowing the quantitation of the PEG portion exposed on the surface of the PEGylated hNPs. While both Ova/CpG_DSPE-PEG@PLGA and Ova/CpG_DSPE-PEG@PLGA/PEI$_{low}$ exhibited ≈80 μg of PEG per mg of hNPs, a lower amount of PEG was quantified for Ova/CpG_DSPE-PEG@PLGA/PEI$_{high}$ hNPs, further corroborating a partial shielding of the PEG surface chains by PEI (Figure 4C).

To gain further knowledge on hNP features relevant for mucosal vaccination, also the amount of MPLA associated to MPLA@PLGA hNPs was quantified. In fact, MPLA is a potent agonist of toll-like receptor 4 (TLR-4), playing a crucial role in the nanovaccine platform, to enhance CD4+ T cell responses and to promote DC maturation.[51] Of note, a percentage of MPLA higher than 60% was found in Ova_MPLA@PLGA, progressively decreasing as the amount of PEI added to the formulation increased (Figure 4D).

3.3. Interactions of Ova/CpG Loaded Lipid@PLGA Hybrid Nanoparticles with the Mucus Barrier

To produce lipid@PLGA hNPs that can be successfully conveyed to the respiratory tract, it is essential that they are muco-inert, i.e., with a poor ability to interact with mucus. Indeed, several

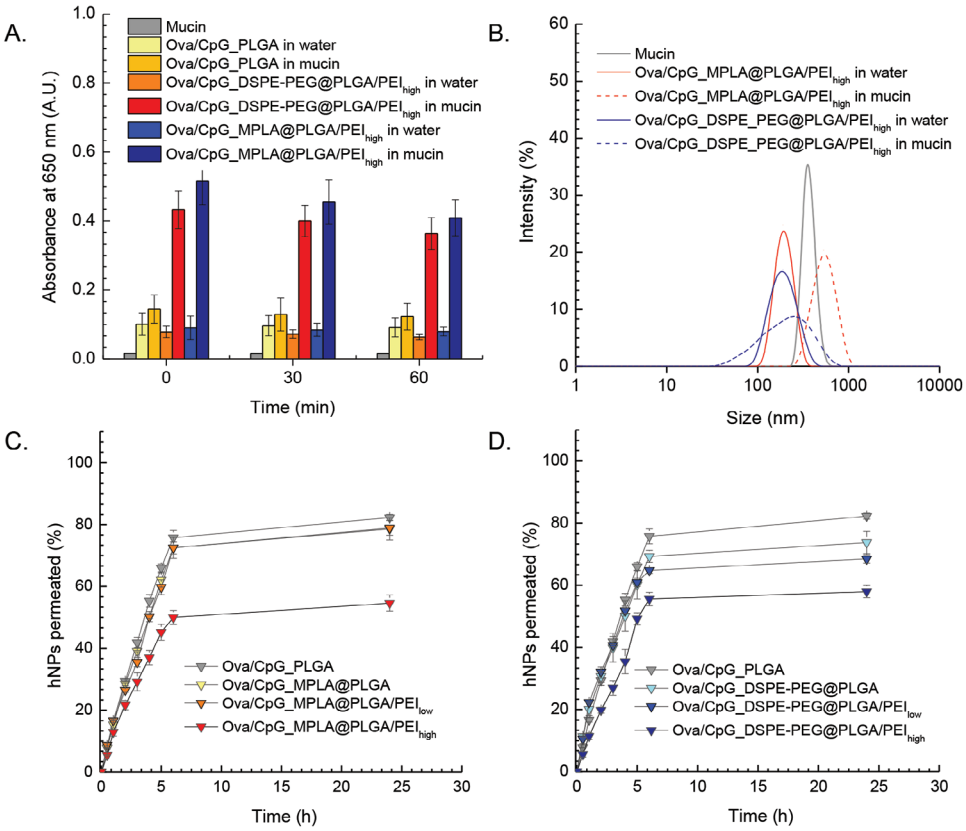

Figure 5. In vitro evaluation of the interactions of Ova/CpG-loaded lipid@PLGA hNPs with the mucus barrier. A) Scattering at 650 nm of hNP/mucin dispersions at time 0 and after incubation for 30 and 60 min at 37 °C. The scattering profile of control hNP dispersions in water and Ova/CpG_PLGA nanoparticles in the same conditions are reported for comparison. B) Size distribution profile of nanoparticle dispersions in water and mucin as evaluated by DLS. C,D) In vitro transport of Ova/CpG-loaded fluorescent hNPs through artificial mucus (AM) as determined by the Transwell® multiplate assay. Results are presented as the percentage of fluorescent hNPs permeating across AM as a function of time. Data are expressed as the mean ± standard deviation (SD) calculated for three different batches (n = 6).

studies have focused on electrostatic and hydrophobic interactions mediated by hydrogen bonds in mucin, which may further reduce the bioavailability of inhaled antigens. For these reasons, nanoparticle/mucin interaction studies were performed as previously reported[30] (**Figure 5**).

Interaction studies showed how the scattering of mucin dispersion is always around zero (0.015-0.035 A.U.), while the addition in the mucin dispersion of positively-charged Ova/CpG-loaded MPLA@PLGA/PEI$_{high}$ and DSPE-PEG@PLGA/PEI$_{high}$ caused a significant increase of the ABS values as compared to their aqueous counterpart (red and blue bars in Figure 5A). Independently upon the presence of mucin in the dispersion, Ova/CpG-loaded PLGA nanoparticles showed approximately constant ABS values, as low as 0.10-0.15 A.U. The results were confirmed by DLS analyses, which clearly showed an increase of the size of PEI$_{high}$ hNP dispersions in mucin with respect to the aqueous ones (Figure 5B). Both the phenomena can be likely ascribed to the absorption of negatively-charged mucin chains on the positive surface of the developed hNPs. In order to investigate whether this phenomenon affected the ability of hNPs to diffuse through the mucus barrier lining the respiratory epithelium, transport studies through artificial mucus (AM) were carried out in vitro by a previously developed Transwell multiplate assay.[31] In the years since, PEGylation has become a mainstay in the formulation of mucus penetrating particles. Here, we observed that MPLA-coated hNPs may allow fast diffusion through the mucus layer. As expected, by increasing the amount of PEI inside the formulation, the transport rate of lipid@PLGA hNPs through mucus decreased (Figure 5C,D). The delay effect of PEI was especially evident for Ova/CpG_MPLA@PLGA/PEI$_{high}$ and Ova/CpG_DSPE-PEG@PLGA/PEI$_{high}$ formulations, with a percent of hNPs permeated at 24 h still within the range of 55–58%. As previously reported for chitosan-coated PLGA nanoparticles,[38,52] mucin adsorbed onto the system may act itself as a shield and mitigate the mechanism of "interaction filtering" preventing drug particles from readily diffusing through mucus gel.

3.4. Insight into Ova/CpG Loaded Lipid@PLGA Hybrid Nanoparticles Structure

Thermoanalytical tests were performed to examine any possible mofication in the crystalline/amorphous behavior and physical properties of the individual components once assembled into the lipid@PLGA hNPs. The DSC analysis was performed firstly on raw PLGA (T_g 50.05 °C), Ova (T_g 73.14 °C) and

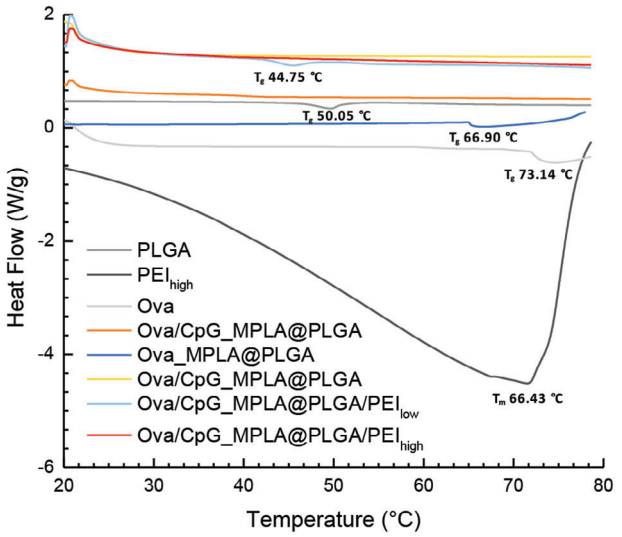

Figure 6. DSC thermograms of MPLA@PLGA hNPs formulations in comparison to PLGA, Ova and PEI as raw materials in the temperature range from 20 to 80 °C at a constant heating rate of 5 °C min^{-1}.

PEI (T_g 66.43 °C), showing a thermodynamic behavior comparable to data reported in literature[53–55] (**Figure 6**). Independently upon the composition, DSPE-PEG@PLGA hNPs did not exhibit any endothermic peak ascribable to components of the formulation (Figure S2, Supporting Information). A characteristic amorphous behavior has been shown also by the formulations Ova/CpG_PLGA, Ova/CpG_MPLA@PLGA, and Ova/CpG_MPLA@PLGA/PEI_{high} considering the absence of any endothermal peak related to the raw materials (Figure 6). The thermogram of the Ova_MPLA@PLGA hNPs shows a slightly shifted endothermal peak (T_g 66.90 °C) (Figure 6). This result suggests the presence of a residual content of Ova not completely molecularly dispersed in the lipid@PLGA matrix if neither CpG nor PEI are included in the formulation, which could explain also the lower entrapment efficiency as compared to PEI-engineered formulations co-encapsulating Ova and CpG. Meanwhile, an early endothermal peak (T_g 44.75 °C), referable to PLGA, occurs in the thermogram of the Ova/CpG_MPLA@PLGA/PEI_{low} hNPs, implying a partial amorphization of the materials during the assembling process and even more decreased crystallinity of the polymer (Figure 6). Of note, this behavior no longer occurs in the case of the corresponding Ova/CpG-loaded PEI_{high} formulations. The collected results suggest that not only the co-presence of Ova, CpG and PEI in the MPLA@PLGA formulations, but also the relative amounts, strongly affect the final architecture of the hNPs, requiring further investigations.

SAXS investigation provided further characterization of the MPLA@PLGA hNPs structure at the nanoscale and can be relevant for a mechanistic understanding of the role that each additional component plays in the assembly process to build the final nanoconstructs. Based on the results described above, the attention was focused on MPLA@PLGA/PEI hNPs: Ova/CpG_MPLA@PLGA/PEI_{low}, Ova/CpG_MPLA@PLGA/PEI_{high} and Ova_MPLA@PLGA/PEI_{high} hNPs, the last missing the CpG payload. **Figure 7A** reports the scattering spectra of the three hNP formulations and their best fit obtained by applying the form factors of multishell spheres with smooth interfaces (radial SLD profiles are reported in Figure 7B). The applied q-vector range addresses distances of 1 to 60 nm in the direct space where the inner features are highlighted while the overall particle size is not visible. However, a core radius of ≈65 nm is confirmed here for all hNPs by the fitting of the first minimum at low q_vector, in agreement with results from TEM, DLS and NTA. The profiles of the two hNPs with high PEI content (red circles and orange squares) show a distinct feature for q above 0.2 nm^{-1}, which is not visible for the low PEI containing hNP (blue triangles). This feature is analyzed as originating from a PEI shell coating the PLGA core. Interestingly, the profiles are very different in presence or absence of CpG, meaning that the nucleic acid cargo can shape the particle structure, despite being of minor relative mass in the formulation. In particular, the scattering profile of Ova_MPLA@PLGA/PEI_{high} shows a single shell of 10 nm thickness, smoothly decreasing in density toward water, while, on the contrary, for Ova/CpG_MPLA@PLGA/PEI_{high} hNPs, where Ova and CpG are co-loaded, the profile reveal a double-shell with a first 2–3 nm denser inner shell and an outer less dense shell of ≈9 nm. The inner shell with higher contrast might originate from the Ova and CpG loads (low relative mass), but necessarily involve relevant amount of PEI or PLGA to get enough intensity to be revealed. The revealed layering of the hNPs outer interface agrees with TEM images that show partially peeled particles suggesting likewise surface stratification (figure 2B). Finally, as already mentioned, the PEI_{low} hNP does not show the extended shell and the slope of the SLD profile smoothly decrease from the electron density of the PLGA core to that of water in a few nanometers distance.

To comprehend the not straightforward differences between Ova/CpG-loaded and Ova-loaded hNPs in SAXS outcomes and, consequently, to make clear the role of CpG and Ova, we performed molecular dynamics (MD) simulations lasting up to 1.3 µs. Interestingly, our simulations demonstrated that Ova and CpG form a stable complex in water, with the nucleic acid interacting with the positive patch on the Ova surface (see Movie S1, Supporting Information). We can speculate that, ones the water phase is put in contact with PEI coming from the oil phase, the strong charge interaction among CpG and PEI might drive to the formation of large and relatively dense assembly with increased contrast. To go further in the mechanistic understanding of the components' arrangement in hNPs, we investigated the behavior of MPLA in the presence of Ova-CpG complex. Four different Ova-CpG complexes were generated by docking (Figure S3, Supporting Information) which after MD converges to a single defined binding mode (**Figure 8A–C**). MPLA molecules were seen to interact with Ova indifferent protein regions, among which close to the CpG binding site (Figure 8C and Movie S2, Supporting Information). This may suggest that the Ova/CpG complex can form stable interactions with the MPLA layer of hNPs, resulting in better stabilization of the complex at the surface of the PLGA core.

SAXS investigation was extended to Ova/CpG_DSPE-PEG@PLGA/PEI_{high} hNP and compared to a previously acquired SAXS spectrum from DSPE-PEG@PLGA hNPs containing low amount of PEI (gray line) (Figure 7C).[26] In line with results achieved with MPLA@PLGA hNPs, the addition of high PEI contents in the formulation confers to Ova/CpG-loaded DSPE-

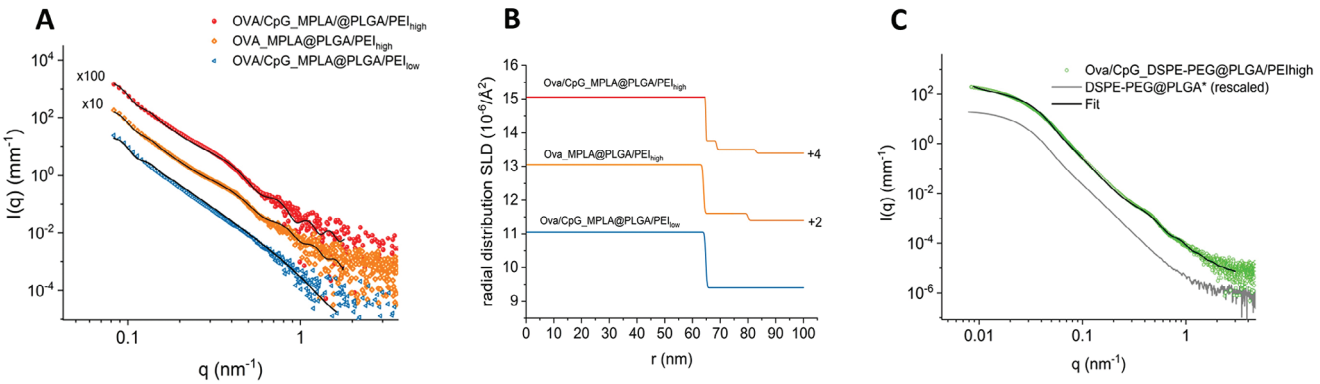

Figure 7. A) SAXS spectra and fitting of high PEI containing, CpG loaded (red circle) or unloaded (orange squares), MPLA@PLGA hNPs and of low PEI containing MPLA@PLGA hNPs (blue triangles). For the sake of visibility, Ova/CpG_MPLA@PLGA/PEIhigh and Ova_MPLA@PLGA/PEIhigh hPNs spectra are shifted by a factor of 100 and 10, respectively. Spectra are analyzed by core-multishell form factor models. Particle radii were polydisperse with PDI = 0.15. Data are acquired at Austrian SAXS beamline of ELETTRA (IT). B) Data are acquired at Austrian SAXS beamline of ELETTRA (IT). B) Radial distribution of the Scattering Length Density for the three particles in A. C) SAXS spectra of Ova/CpG_DSPE-PEG@PLGA/PEIhigh hNPs (green circles) with a core-multishell form factor fit (black line) in comparison with the scattering profile of DSPE-PEG@PLGA hNPs (gray line / rescaled). Data are acquired at the beamline ID02 of ESRF (FR). (*) previously studied.[26]

PEG@PLGA hNPs a featuring of the spectrum at ≈0.4 nm^{-1} (red line in Figure 7C), which is not visible in the presence of only PEG at interface (gray line in Figure 7C). The fit indicates the presence of a diffuse shell of ≈13 nm of increasing contrast, likely ascribed to PEI interacting with PEG chains at the hNPs surface by strong hydrogen bonds, in agreement with literature data.[56,57]

3.5. In Vitro Evidence of Lipid@PLGA Hybrid Nanoparticles Uptake in Murine Dendritic Cells and Antigen Cross-Presentation Efficiency

Selected formulations were tested for: i) uptake studies on murine dendritic cells (BM-DCs), ii) antigen presentation tests to B3Z OT-I hybridoma cells expressing a TCR that specifically recognize the Ova (257–264) peptide (SIINFEKL).

Cross-presentation represents the presentation of exogenous antigens by MHCI and influence the outcome of CD8+ T cell response in recognising and killing cells infected by virus, intracellular parasites or tumoral cells. Efficient cross-presentation is a major goal for vaccine formulations able to induce cell mediate immune response.

Selected formulations were tested for their ability to be taken up by BM-DCs, that are professional antigen-presenting cells, and to induce antigen cross-presentation. The antigen uptake and intracellular localization/trafficking were investigated by immunofluorescence and confocal laser scanning microscopy (**Figure 9**). To visualize nanoparticles' uptake by BM-DCs, cells were incubated with the Ova/CpG loaded lipid@PLGA hNPs for

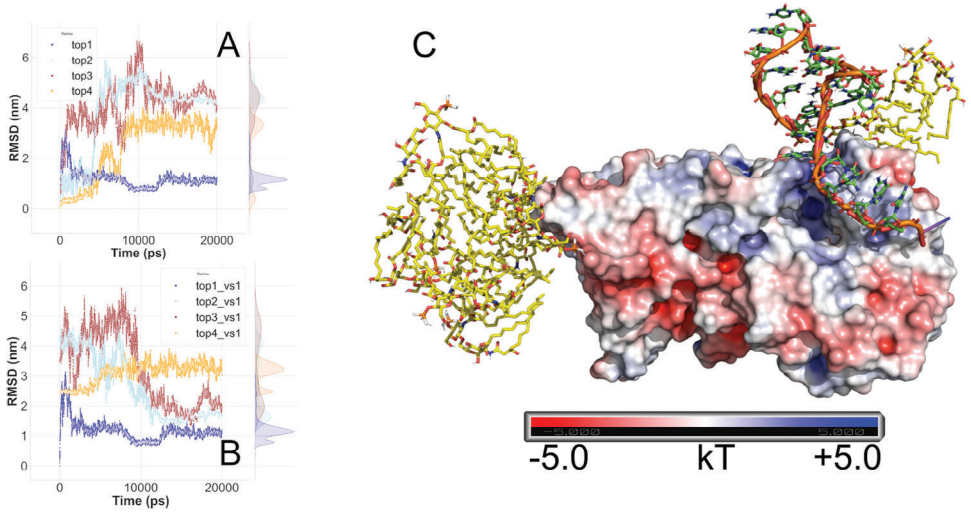

Figure 8. Molecular dynamics simulations of Ova/CpG_MPLA system. A) RMSD time series of 4 different replica Ova/CpG calculated on P-DNA atoms with respect to docking output. B) RMSD time series of 4 different replicas of Ova/CpG_MPLA calculated on P-DNA atoms with respect to top 1 C) 3D model structure Ova/CpG_MPLA of top1 after 200 ns of simulations. Ova proteins is represented as electrostatic surface ±5kT, CpG as brown cartoon and green sticks, MPLA molecules as yellow (fatty acyl group) and red licorice (sugar oxygen).

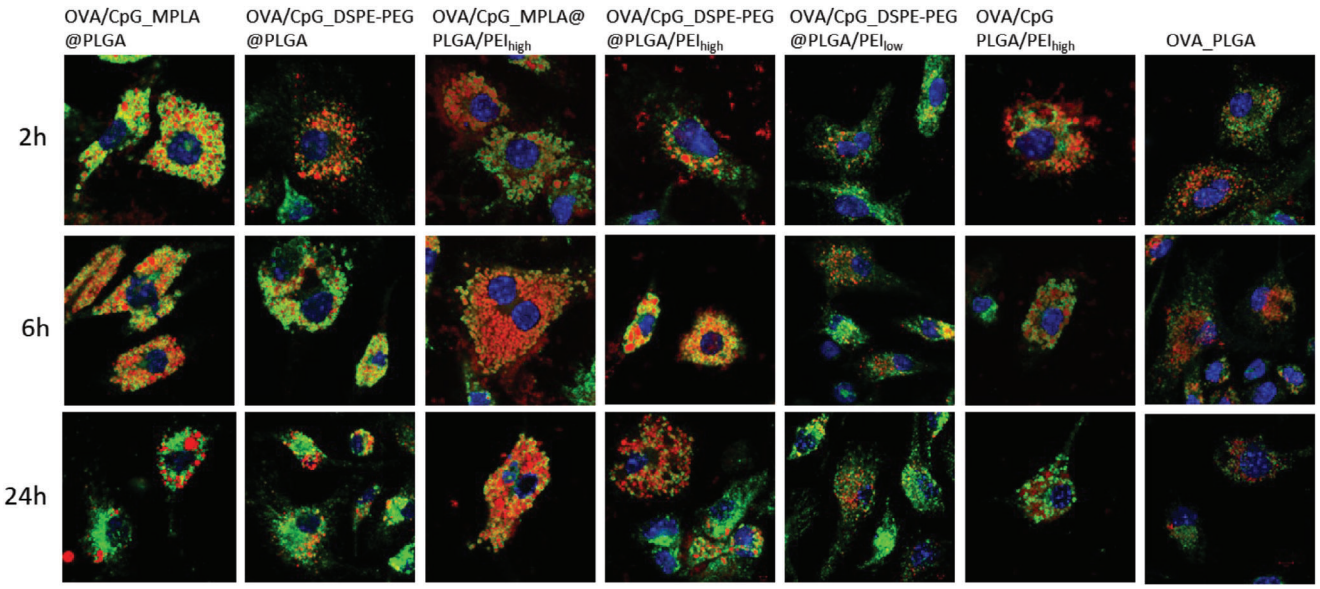

Figure 9. *Antigen uptake and cross-presentation*. In vitro uptake of rhodamine-labeled hNPs (red) in murine DCs (green: LAMP-1, lysosomal marker), cell nuclei are stained blue with Hoechst. Representative color overlay images for 2, 6, and 24 h time points are shown.

three different time points (2, 6, and 24 h) at the concentration 10 μg ml^{-1}. These time points were chosen in order to assess cell-entry kinetic and intracellular half-life and persistence of hNPs. Studies were conducted using fluorescent Ova-loaded hNPs to directly visualize the uptake process and track nanoparticle intracellular trafficking. Fluorescence microscopy analysis showed that all the selected nanoparticles can promptly enter the cell (2 h) and persist (24 h). The analysis of immunofluorescent labeled compartments showed that after 2 h of incubation, Ova/CpG_MPLA@PLGA, Ova/CpG_MPLA@PLGA/PEI_{high}, Ova /CpG_DSPE-PEG@PLGA/PEI_{high} and OVA/CpG-PLGA/PEI_{high} colocalized with a lysosome marker (LAMP-1), while Ova/CpG_DSPE-PEG@PLGA colocalized with LAMP-1 later on (6 h). Of note, representative PEI_{low} formulation (Ova /CpG_DSPE-PEG@PLGA/PEI_{low}) and bare OVA-PLGA nanoparticles never colocalized with LAMP-1 at the time points analyzed. Analysis of images acquired using confocal microscopy suggested that the three PEI_{high} hNPs (i.e., Ova/CpG_MPLA@PLGA/PEI_{high}, Ova/CpG_DSPE-PEG@PLGA/PEI_{high}, Ova/CpG_PLGA/PEI_{high}) are able to entry into endosome-lysosome pathway, as demonstrated *by a* peak of colocalization with LAMP-1 at 2 h, and after that the decreased signal of colocalization showed that these NPs were released into cytoplasm (24 h), probably escaping the lysosome degradation. The lysosome degradation escape is the first step for antigen cross-presentation.[58]

It has well described that extracellular antigens can be presented on MHC-I molecules through endosome-to-cytosol pathway,[59] and according to the proton sponge hypothesis,[60] the buffering capacity of PEI leads to osmotic swelling and rupture of lysosomes with extracellular antigen release into cytoplasm where it can be loaded into MHC-I groove.

Moreover, to measure the antigen presentation, BM-DCs were preincubated over night with the hNPs and the B3Z hybridoma cells were added for 40 h of co-culture. We measured the B3Z cell response to the OVA antigen, as result of Ovalbumin uptake, processing and presentation in the MHCI groove. The B3Z hybridoma cells are specifically activated by OVA antigen, and after TCR engagement the IL-2 gene transcription is activated, resulting in production of IL-2.

As reported in **Figure 10**, we measured, by ELISA assay, the IL-2 production after engulfment and processing of Ova/CpG_MPLA@PLGA/PEI_{high}, Ova/CpG_DSPE-PEG@PLGA/PEI_{high} and Ova/CpG_PLGA/PEI_{high} formulations in a dose-response way, while no IL-2 production was detected when the same formulations, but produced without PEI, were used.

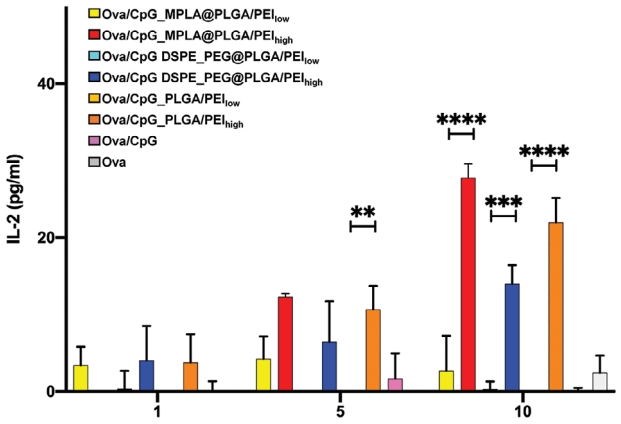

Figure 10. *Antigen cross-presentation*. IL-2 production after B3Z cell activation by antigen-loaded BMDC. 1, 5 and 10 μg ml^{-1} Ovalbumin loaded on different nanoparticle formulations were assayed. IL-2 was measured by ELISA assay; each value represents average (± standard deviation) value of technical replicates. A representative experiment is reported.

4. Conclusions

Pursuing our goal to design and develop a multimodal nanovaccine for the co-delivery of Ova, as model antigen, and CpG motifs as adjuvant, we explored the potential of hNPs comprising a PLGA core surface-engineered with different moieties for the mucosal administration route. If engineering with DSPE-PEG would allow to achieve mucus-penetrating hNPs, the addition of MPLA could at least in principle help to obtain both a mucoinert and immuno-responsive nanoplatform. However, data have shown that polyethyleneimine (PEI), originally included in the nanoplatforms for its ability to improve the efficiency of conventional vaccines against infections and tumors, is the real gamechanger. PEI played a role of paramount importance in promoting the antigen escape from lysosomes and enhancing antigen cross-presentation. Nonetheless, the presence of PEI not only affected the interaction of hNPs with the biological environment, but also the way all the components are assembled during the hNP formation. Indeed, if an interaction CpG/PEI was foreseeable, results suggest that the nucleic acid can interact also with the positive patch on the Ova surface. The consequent synergy between Ova and CpG in engaging with branched PEI causes a rearrangement of the moieties in the final architecture of the hNPs, further contributed by MPLA molecules likely interacting with Ova. Finally, the collected results pave the way to a new concept for mucosal vaccination relying on multicomponent PEI MPLA@PLGA hNPs, stressing the idea that not only the components but the relative amounts are pivotal to tune the nanoparticle features and, in so doing, the way they engage with the biological environment.

Supporting Information

Supporting Information is available from the Wiley Online Library or from the author.

Acknowledgements

This work was supported by PRIN 20173ZECCM_004-NanoTechVax, financed by the Italian Minister of University and Research (MUR). The authors thank the staff of Austrian SAXS beamline at ELETTRA (Trieste, Italy) and of ID02 SAXS beamline at ESRF (Grenoble, France) for support.

Open access publishing facilitated by Universita degli Studi di Napoli Federico II, as part of the Wiley - CRUI-CARE agreement.

Conflict of Interest

The authors declare no conflict of interest.

Data Availability Statement

The data that support the findings of this study are available from the corresponding author upon reasonable request.

Keywords

antigen presentation, lipid/polymer hybrid nanoparticles, mucosal vaccination, PLGA, poly(ethylenimine)

Received: August 2, 2024
Revised: August 29, 2024
Published online:

[1] J. Bessa, N. Schmitz, H. J. Hinton, K. Schwarz, A. Jegerlehner, M. F. Bachmann, *Eur. J. Immunol.* **2008**, *38*, 114.
[2] F. Dotiwala, A. K. Upadhyay, *Vaccines* **2023**, *11*, 1585.
[3] C. J. Y. Tsai, J. M. S. Loh, K. Fujihashi, H. Kiyono, *Expert Rev. Vaccines* **2023**, *22*, 885.
[4] S. Hellfritzsch, *Pharmaceutics* **2019**, *11*, 375.
[5] M. Y.-T. Chow, J. K. W. Lam, in **2023**, *Respiratory Delivery of Biologics, Nucleic Acids, and Vaccines* (Eds.: J. Lam, P. C. L. Kwok), Springer International Publishing, Cham, 123.
[6] E. C. Lavelle, R. W. Ward, *Nat. Rev. Immunol.* **2022**, *22*, 236.
[7] C. Czerkinsky, F. Anjueie, J. R. McGhee, A. Geoige-Chundy, J. Holmgren, M. Kieny, K. Fujiyashi, J. F. Mestecky, V. Pierrefite-Carle, C. Rusk, J. Sun, *Immunological Reviews* **1999**, *170*, 197.
[8] N. K. Al-Nemrawi, R. S. Darweesh, L. A. Al-shriem, F. S. Al-Qawasmi, S. O. Emran, A. S. Khafajah, M. A. Abu-Dalo, *Polymers* **2022**, *14*, 4450.
[9] W. Tang, Y. Zhang, G. Zhu, *Nanoscale* **2022**, *14*, 263.
[10] D. Horvath, M. Basler, *Pharmaceutics* **2023**, *15*, 615.
[11] S. Haque, C. W. Pouton, M. P. McIntosh, D. B. Ascher, D. W. Keizer, M. R. Whittaker, L. M. Kaminskas, *Nanomedicine: Nanotechnology, Biology and Medicine* **2020**, *30*, 102291.
[12] R. Scherließ, J. Janke, *Pharmaceutics* **2021**, *13*, 1196.
[13] C. Thomas, A. Rawat, L. Hope-Weeks, F. Ahsan, *Mol. Pharmaceutics* **2011**, *8*, 405.
[14] M. Kabiri, M. Sankian, K. Sadri, M. Tafaghodi, *Eur. J. Pharm. Biopharm.* **2018**, *133*, 321.
[15] V. Schijns, A. Fernández-Tejada, Ž. Barjaktarović, I. Bouzalas, J. Brimnes, S. Chernysh, S. Gizurarson, I. Gursel, Ž. Jakopin, M. Lawrenz, C. Nativi, S. Paul, G. K. Pedersen, C. Rosano, A. Ruiz-de-Angulo, B. Slütter, A. Thakur, D. Christensen, E. C. Lavelle, *Immunological Reviews* **2020**, *296*, 169.
[16] P.-Y. Chou, S.-Y. Lin, Y.-N. Wu, C.-Y. Shen, M.-T. Sheu, H.-O. Ho, *J. Controlled Release* **2022**, *351*, 970.
[17] E. Zupančič, C. Curato, M. Paisana, C. Rodrigues, Z. Porat, A. S. Viana, C. A. M. Afonso, J. Pinto, R. Gaspar, J. N. Moreira, R. Satchi-Fainaro, S. Jung, H. F. Florindo, *J. Controlled Release* **2017**, *258*, 182.
[18] M. Ebrahimian, M. Hashemi, M. Maleki, G. Hashemitabar, K. Abnous, M. Ramezani, A. Haghparast, *Front. Immunol.* **2017**, *8*, 1077.
[19] B. Li, M. Siuta, V. Bright, D. Koktysh, B. Matlock, M. Dumas, M. Zhu, A. Holt, D. Stec, S. Deng, P. Savage, S. Joyce, W. Pham, *IJN* **2016**, *11*, 6103.
[20] S. T. Jahan, S. M. A. Sadat, M. Yarahmadi, A. Haddadi, *Mol. Pharmaceutics* **2019**, *16*, 498.
[21] K. A. Fitzgerald, J. C. Kagan, *Cell* **2020**, *180*, 1044.
[22] K. L. Wilson, G. P. Howard, H. Coatsworth, R. R. Dinglasan, H.-Q. Mao, M. Plebanski, *Vaccines* **2020**, *8*, 261.
[23] B. Slütter, S. Bal, C. Keijzer, R. Mallants, N. Hagenaars, I. Que, E. Kaijzel, W. Van Eden, P. Augustijns, C. Löwik, J. Bouwstra, F. Broere, W. Jiskoot, *Vaccine* **2010**, *28*, 6282.
[24] P. Gu, A. Wusiman, S. Wang, Y. Zhang, Z. Liu, Y. Hu, J. Liu, D. Wang, *Carbohydr. Polym.* **2019**, *223*, 115128.
[25] C. Liu, X. Jiang, Y. Gan, M. Yu, *Medicine in Drug Discovery* **2021**, *12*, 100110.
[26] G. Conte, G. Costabile, D. Baldassi, V. Rondelli, R. Bassi, D. Colombo, G. Linardos, E. V. Fiscarelli, R. Sorrentino, A. Miro, F. Quaglia, P. Brocca, I. d'Angelo, O. M. Merkel, F. Ungaro, *ACS Appl. Mater. Interfaces* **2022**, *14*, 7565.
[27] C. Shen, J. Li, Y. Zhang, Y. Li, G. Shen, J. Zhu, J. Tao, *IJN* **2017**, *12*, 5443.

[28] G. Wang, H. Zhou, Q.-G. Nian, Y. Yang, C.-F. Qin, R. Tang, *Chem. Sci.* **2016**, *7*, 1753.
[29] A. Alloatti, F. Kotsias, E. Hoffmann, S. Amigorena, *BIO-PROTOCOL* **2016**, *6*.
[30] B. Casciaro, I. d'Angelo, X. Zhang, M. R. Loffredo, G. Conte, F. Cappiello, F. Quaglia, Y.-P. P. Di, F. Ungaro, M. L. Mangoni, *Biomacromolecules* **2019**, *20*, 1876.
[31] I. d'Angelo, G. Costabile, E. Durantie, P. Brocca, V. Rondelli, A. Russo, G. Russo, A. Miro, F. Quaglia, A. Petri-Fink, B. Rothen-Rutishauser, F. Ungaro, *J. Aerosol Med. Pulmon. Drug Del.* **2018**, *31*, 170.
[32] C. Conte, P. F. Monteiro, P. Gurnani, S. Stolnik, F. Ungaro, F. Quaglia, P. Clarke, A. Grabowska, M. Kavallaris, C. Alexander, *Nanoscale* **2021**, *13*, 11414.
[33] C. Conte, I. Fotticchia, P. Tirino, F. Moret, B. Pagano, R. Gref, F. Ungaro, E. Reddi, C. Giancola, F. Quaglia, *Colloids Surf., B* **2016**, *141*, 148.
[34] F. Ungaro, G. De Rosa, A. Miro, F. Quaglia, *J. Pharm. Biomed. Anal.* **2003**, *31*, 143.
[35] S. Michael, *SAXSutilities2: a graphical user interface for processing and analysis of Small-Angle X-ray Scattering data*, Zenodo, **2021**.
[36] I. Breßler, J. Kohlbrecher, A. F. Thünemann, *J. Appl. Crystallogr.* **2015**, *48*, 1587.
[37] L. A. Feigin, D. I. Svergun, *Structure Analysis by Small-Angle X-Ray and Neutron Scattering* (Ed.: G. W. Taylor), Springer US, Boston, MA, **1987**.
[38] I. d'Angelo, B. Casciaro, A. Miro, F. Quaglia, M. L. Mangoni, F. Ungaro, *Colloids Surf., B* **2015**, *135*, 717.
[39] G. Costabile, I. d'Angelo, G. Rampioni, R. Bondì, B. Pompili, F. Ascenzioni, E. Mitidieri, R. d'Emmanuele di Villa Bianca, R. Sorrentino, A. Miro, F. Quaglia, F. Imperi, L. Leoni, F. Ungaro, *Mol. Pharmaceutics* **2015**, *12*, 2604.
[40] M. Schlich, L. D'Apice, F. Lai, C. Sinico, D. Valenti, F. Catalano, R. Marotta, P. Decuzzi, P. Italiani, A. M. Fadda, *Int. J. Pharm.* **2024**, *661*, 124404.
[41] R. Sartorius, L. D'Apice, P. Barba, D. Cipria, L. Grauso, A. Cutignano, P. De Berardinis, *Front. Immunol.* **2018**, *9*, 1496.
[42] H. Shen, A. L. Ackerman, V. Cody, A. Giodini, E. R. Hinson, P. Cresswell, R. L. Edelson, W. M. Saltzman, D. J. Hanlon, *Immunology* **2006**, *117*, 78.
[43] G. Costabile, G. Conte, S. Brusco, P. Savadi, A. Miro, F. Quaglia, I. d'Angelo, F. Ungaro, *Pharmaceutics* **2024**, *16*, 347.
[44] J. S. Suk, Q. Xu, N. Kim, J. Hanes, L. M. Ensign, *Adv. Drug Delivery Rev.* **2016**, *99*, 28.
[45] E. Fröhlich, *IJN* **2012**, 5577.
[46] S. Salatin, A. Yari Khosroushahi, *J Cellular Molecular Medi* **2017**, *21*, 1668.
[47] F. Ungaro, G. De Rosa, F. Quaglia, E. Fattal, M. I. La Rotonda, *J. Drug Deliv. Sci. Technol.* **2005**, *15*, 137.
[48] J. Nam, S. Son, K. S. Park, J. J. Moon, *Adv. Sci.* **2021**, *8*, 2002577.
[49] J. Xu, K. Wan, H. Wang, X. Shi, J. Wang, Y. Zhong, C. Gao, Y. Zhang, G. Nie, *ACS Cent. Sci.* **2021**, *7*, 1938.
[50] J. R. Endres, I. Qureshi, T. Farber, J. Hauswirth, G. Hirka, I. Pasics, A. G. Schauss, *Food Chem. Toxicol.* **2011**, *49*, 1174.
[51] C. Pifferi, R. Fuentes, A. Fernández-Tejada, *Nat Rev Chem* **2021**, *5*, 197.
[52] F. Ungaro, I. d' Angelo, A. Miro, M. I. La Rotonda, F. Quaglia, *J. Pharm. Pharmacol.* **2012**, *64*, 1217.
[53] S. Photchanachai, A. Mehta, N. Kitabatake, *Biosci., Biotechnol., Biochem.* **2002**, *66*, 1635.
[54] M. M. Mady, *Int. J. Phys. Sci.* **2011**, *6*.
[55] G. Liu, K. McEnnis, *Polymers* **2022**, *14*, 993.
[56] T. Vasiliu, B. F. Craciun, A. Neamtu, L. Clima, D. L. Isac, S. S. Maier, M. Pinteala, F. Mocci, A. Laaksonen, *Biomater. Sci.* **2021**, *9*, 6623.
[57] J. Li, Y. Du, H. Su, S. Cheng, Y. Zhou, Y. Jin, X.-R. Qi, *Acta Pharm. Sin. B* **2020**, *10*, 1122.
[58] J. M. Blander, *Annu. Rev. Immunol.* **2018**, *36*, 717.
[59] J. M. Blander, K. J. Yee Mon, A. Jha, D. Roycroft, *Adv. Immunol.* **2023**, *159*, 33.
[60] R. V. Benjaminsen, M. A. Mattebjerg, J. R. Henriksen, S. M. Moghimi, T. L. Andresen, *Mol. Ther.* **2013**, *21*, 149.